Control of Cavity Flow Oscillations by High Frequency Forcing

M. A. Martinez
G. M. Di Cicca
M. Iovieno
M. Onorato

DIASP, Politecnico di Torino,
Corso Duca degli Abruzzi,
24, 10129 Torino, Italy

Time resolved two-dimensional particle image velocimetry (2DPIV) experiments have been conducted to contribute to the understanding of the physics governing the suppression mechanism of cavity flow self-sustained oscillations by means of high frequency excitation of the cavity shear layer. High frequency excitation was introduced by the spanwise coherent vortex shedding in the wake of a cylindrical rod positioned just upstream the cavity entrance, at the edge of the incoming boundary layer. The effectiveness of this suppression was demonstrated for a cavity having the length-to-depth ratio equal to three, in incompressible flow. The spatial and time resolved PIV measurements of the whole flow field in the plane normal to the cavity floor, linear stability analysis of the measured shear layer mean velocity profiles, and preliminary PIV measurements in a plane parallel to the cavity allowed us to offer a better insight into the involved physical mechanisms in suppressing cavity self-sustained oscillations. [DOI: 10.1115/1.4006468]

Introduction

Cavity flows arise in many aerospace, automotive, industrial, and environmental applications. Under specific conditions the presence of the cavity generates self-sustained oscillations producing narrow-band pressure and velocity fluctuations.

The physical process leading to self-sustained oscillations of the flow cavity at high subsonic flow was evidenced by Rossiter [1]. Vortical instabilities in the shear layer separating from the cavity leading edge are amplified as they are convected downstream. Upon interacting with the downstream wall of the cavity, they generate pressure waves which propagate upstream. Receptivity at the upstream edge of the cavity triggers the vortex shedding and regulates the feedback loop. In [1] Rossiter also developed a semiempirical formula to predict the cavity self-sustained oscillation frequencies when the geometrical and physical characteristics of the cavity allow them to occur:

$$\mathrm{St} \equiv \frac{fL}{u_e} = \frac{n-\gamma}{\mathrm{M}+1/k}$$

where St is the Strouhal number based on the cavity length L and on the undisturbed velocity u_e, f is the frequency, n is the integer mode number, M is the Mach number, k is the ratio of the convection velocity of the structures in the shear layer to the free-stream velocity, and γ is an empirical constant. As suggested by Rossiter [1], $k=0.57$ and $\gamma=0.25$. For high subsonic flow most of the experimental results are in agreement with the Rossiter formula, but at very low Mach number a large scatter in the distribution of the Strouhal numbers for similar conditions are observed, and some results deviate from Rossiter model.

The important parameters for the flow configuration in a rectangular cavity are the ratios L/H, L/W, and L/θ, where H,W, and θ are, respectively, the cavity depth, width, and the upstream boundary layer momentum thickness, and the flow parameters M_∞, δ^*/θ, Re_θ, and $p_{\mathrm{rms}}/q_\infty$. δ^* is the displacement thickness of the upstream boundary layer, p is the pressure, p_{rms} is the root mean square of the fluctuating pressure, and q_∞ is the free-stream dynamic pressure.

Gharib and Roshko [2] identified two oscillation modes in laminar cavity flows, which they denoted "shear layer mode" and "wake mode." When the ratio of the cavity length to the incoming boundary-layer momentum thickness L/θ exceeds 80, the self-sustained oscillations are in the shear layer mode. When the ratio exceeds 120, however, the oscillations shift to the wake mode, causing an abrupt increase in the drag. Sarohia [3] found that for a laminar incoming boundary layer the self-sustained oscillations occur under the criterion of $L/\delta(\mathrm{Re}_\delta)^{1/2} \geq 290$, where δ is the thickness of the incoming boundary layer, and the oscillating frequency jumps to a higher mode as the cavity length increases.

Independently from the generation mechanisms, cavity self-sustained oscillations, when they occur, produce high amplitude discrete tones in the pressure (and velocity) spectrum, at well-defined frequencies, that can lead to structural vibration, intense noise radiation, and increases in mean drag. Moreover, coupling between flow oscillations and wall cavity structures may develop condition of resonance, leading quickly to structural fatigue issues.

An important challenge is then to suppress these large-amplitude oscillations with the smallest actuator requirements [4]. Passive actuators, as leading edge ramps, spoilers, fences, and contouring the trailing and/or the leading edges of the cavity have been successfully tested and some of them applied. They may reduce the discrete tones by shifting the shear layer reattachment region downstream of the cavity edge, or by modifying the stability characteristic of the shear layer velocity profile, or by disrupting the shear layer spanwise coherence.

Active open-loop and closed-loop control devices, having as objective the disruption of the Rossiter feedback loop, have been also successfully tested. Examples of such devices include oscillating electromechanical and piezoelectric flaps, steady and pulsed blowing, voice-coil drivers, powered resonance tubes, fluidic oscillating jets, and synthetic jets. Cattafesta et al. [5] and Rowley and Williams [4] provide extensive reviews and complete reference indications of such cavity flow control techniques.

Passive actuators attenuate tones requiring the least expensive and least complicated devices; however, they often do not work well at off-design conditions. Active open-loop devices are attractive for their ability to be activated when needed. They are energy consuming devices and, like passive actuators, they must be optimized for each flow condition. Active closed–loop devices have the potential for greater reduction in the cavity tones with much less power requirement and drag penalty than passive or active open-loop techniques. In addition, closed-loop control is generally

Contributed by the Fluids Engineering Division of ASME for publication in the JOURNAL OF FLUIDS ENGINEERING. Manuscript received July 29, 2011; final manuscript received March 22, 2012; published online May 3, 2012. Assoc. Editor: Olivier Coutier-Delgosha.

less sensitive to changes in operating conditions and can be adjusted, for example, to flight conditions. Unlikely, complexity and cost are typically increased since one or more sensors and accurate dynamic models are required to operate the closed-loop control.

A typical approach for active flow control is to manipulate the flow by an external forcing at a frequency of the same order of magnitude of the system oscillation frequency. In these conditions the growth of some oscillation modes can be suppressed.

It has been demonstrated that individual tones can be completely suppressed and also overall sound pressure levels may be considerably reduced by forcing the cavity shear layer at a frequency about one order of magnitude (or more) higher than the cavity self-sustained oscillation frequency. High frequency forcing was first introduced by McGrath and Shaw [6], using, as forcing device, the vortices shed from a cylinder in cross flow at the cavity leading edge, placed in the upstream subsonic boundary layer. Extensive studies using cylinders were afterward done, among others, by Shaw [7], Stanek and co-workers [8–10], Smith et al. [11], Ukeiley et al. [12], and Panickar and Raman [13]. All of these authors have proven the effectiveness in reducing or suppressing tones and in reducing the broadband spectrum by introducing high frequency disturbances into the shear layer separating from the cavity leading edge.

Although it has been demonstrated the effectiveness of this high frequency forcing, there is a lack of clear understanding of the physics driving the suppression mechanism. It is necessary to understand the physics governing this resonance suppression mechanism in order to optimize actuator design for achieving maximum suppression performance. Several hypotheses to explain the tone suppression have been proposed. In the early work of McGrath and Shaw [6] emphasis was given to the direct interaction of the shed vortices by the rod in cross flow with the shear layer instability. Stanek et al. [8] attributed the suppression by high frequency forcing to an accelerated energy cascade in the conservative part of the energy spectra, stimulated by the excitation. This accelerated cascade is accompanied by the elimination of all large coherent structures in the shear layer, reduction in the size of the smallest identifiable coherent structures, and increase of the viscous dissipation rate. Ukeiley et al. [12] presented experimental evidence that the cylinder lifts the shear layer and causes the impingement region to be altered, affecting the pressure wave source region and consequently interrupting the Rossiter feedback loop responsible for the cavity self-sustained oscillation phenomenon. Furthermore, Stanek et al. [9] offered a new model for high frequency forcing. They stated that high frequency forcing alters the stability characteristics of the mean flow in the shear layer such that the growth of the large scale disturbances is inhibited or prevented.

More recently, Stanek et al.'s [10] numerical simulation shows that the initial spanwise coherence and the successive breakdown of the pair of opposite sign vortical structures produced by the rod lead to a dramatic reorganization of the vorticity field in the shear layer. The authors argue that this specific vorticity reorganization is responsible for the observed stabilization, leading to the tone suppression. Panickar and Raman [13], on the basis of measurements in the shear layer and linear stability calculations based on experimental data, proposed a new model to explain cavity self-sustained oscillation suppression using high frequency excitation. According to this model, the suppression is brought about by introducing high frequency excitation into the shear layer. This excitation frequency has to be high enough to lie outside the envelope of amplified instabilities such that a dominant part of the energy of the excited flow in the shear layer is contained within this frequency. This spanwise coherent, high frequency excitation introduced by the rod in cross flow just upstream the cavity leading edge decays rapidly as it is convected downstream along the shear layer. Later, Sarpotdar et al. [14] demonstrated that the link between the cavity tone suppression and the influence of the cylinder on the shear layer stability is weak. They stated also that other mechanisms for cavity resonance suppression using the cylinder in cross-flow configuration, such as high frequency forcing and shear layer lift-off, will need to be examined more closely before a conclusive statement can be made.

The primary objective of the current work was to conduct a fundamental time resolved 2DPIV experiment in the wall normal plane of a shallow rectangular cavity, having the ratio length/depth $L/H = 3$, with laminar incoming boundary layer, subject to external high frequency forcing. The goal of the work was to contribute to the understanding of the physics governing the suppression mechanism of cavity flow large amplitude tones by means of the high frequency excitation of the shear layer. It should be considered that a better understanding of this control mechanism is also of great interest for the general approach of flow control in complex systems. In addition, time resolved PIV allows giving complete boundary layer, shear layer, and cavity internal flow measurements of mean and fluctuating flow components and allows characterizing completely the interaction between the control device and the flow.

Experimental Setup

Planar PIV time-resolved experiments were carried out in a water tunnel, 350×350 mm^2 test section, at the Politecnico di Torino. Figure 1 shows the cavity model in the tunnel test section. The cavity depth H was 10 mm, the cavity length-to-depth ratio was $L/H = 3$. The center of the cylindrical transverse rod was positioned at $x/H = -0.5$ and $y/H = 0.5$. The rod diameter d was 0.8 mm.

PIV measurements were taken in the streamwise plane normal to the cavity floor, at the cavity midspan. A preliminary PIV measurement was also done in a plane parallel to the cavity floor at $y/H = 0.05$.

The PIV system was composed by a Spectra-Physics Argon-Ion cw laser with a maximum emitted beam power of 6 W and a Dantec MKIII CMOS camera with a resolution of 1280×1024 pixels and a maximum recording rate at full resolution of 1000 fps. The flow was seeded with hollow glass spheres with a nominal diameter of 10 μm. The laser light sheet was about 1 mm thick.

Two successive images were cross correlated to obtain the velocity field using a multigrid algorithm provided by the DAVIS 7.2 software from LaVision, with an initial interrogation window size of 128×128 pixels and a final interrogation window size of 32×32 pixels, with a 50% overlap. Subpixel refinement and window deformation were applied. The spatial resolution of the measurement was 0.8×0.8 mm^2.

All the PIV measurements were performed at the frequency of 1000 Hz. The exposure time of each PIV image was 190 μs. The

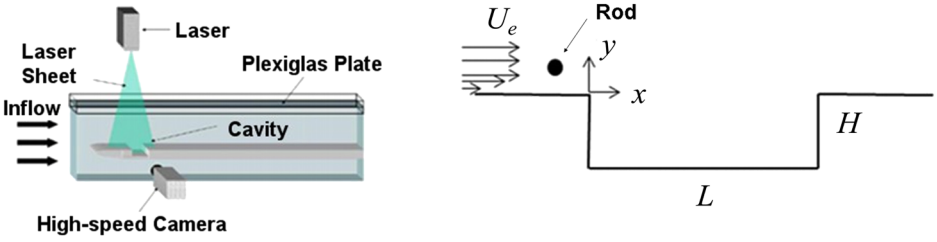

Fig. 1 Experimental setup

Table 1 Experimental conditions for the cavity flow

u_e	δ	θ	δ^*/θ	Re_θ	Re_L	L/θ
0.31 m/s	2.3 mm	0.37 mm	2.36	113	9300	81

camera has an internal memory of 4GB, which limited the acquisition time to 3.2 s, giving 3200 images. In order to perform statistics using uncorrelated (statistically independent) data, only two consecutive images every 100 images were memorized; thus an effective acquisition rate of 10 Hz was performed. The number of acquired image pairs for the statistics was 3000. The images for the time resolved analysis and for the spectral analysis were memorized at the full frequency of 1000 Hz. The spectra were averaged on six packages of 3200 images each.

The uncertainty in measuring the velocity with PIV depends mainly on the quality of the images, the particle image size, the particle image density, the displacement of the particles from one image to the successive, and the velocity gradient. Since the particle image size was 2–3 pixels and a good contrast between the particle light intensity and the background light intensity was obtained, the error in locating the correlation peak was estimated to be lower than 0.1 pixels (see [15]). Taking into account a displacement of particles from the first to the second image of about 12 pixels in the outer flow and about half of it in the shear layer, the error in measuring the instant velocity is less than 2%.

The experimental conditions for the baseline (noncontrolled) flow are listed in Table 1, where u_e is the external undisturbed flow velocity. The Reynolds number $\mathrm{Re}_L = u_e L/\nu$ was 9300. The Reynolds number $\mathrm{Re}_\theta = u_e\theta/\nu$ was 113. The ratio L/θ was 81, which is just above the $L/\theta = 80$ threshold for the onset of self-sustained cavity oscillations, as determined by Gharib and Roshko [2]. The criterion reported in Sarohia [3] to occur self-sustained oscillations for a laminar incoming boundary layer $L/\delta(\mathrm{Re}_\delta)^{1/2} \geq 290$ is also satisfied. Namely, in the present experiment $L/\delta(\mathrm{Re}_\delta)^{1/2} = 348$.

The controlled flow experiments were carried out at same flow conditions. The vortex shedding frequency from the rod was $f = 77.5$ Hz ($\mathrm{St} \equiv f\ L/u_e = 7.5$), about one order of magnitude higher than the cavity self-sustained oscillation frequency expected for the baseline flow.

In Fig. 2 the boundary layer velocity profiles at the cavity leading edge ($x = 0$) are reported for the baseline and for the controlled flows and compared with the theoretical Blasius velocity profile for a laminar flow. For the present experimental conditions the incoming boundary layers appear to be laminar. The velocity defect due to the rod wake is evident in the case of the controlled flow. The rod appears situated well outside the incoming boundary layer. It should here reported that Sarpotdar et al. [14] conducted a parametric study to optimize the gap g between the rod and the cavity wall, founding the optimum gap to be $g/\delta = 1.14$. In the present experiment $g/\delta = 2$.

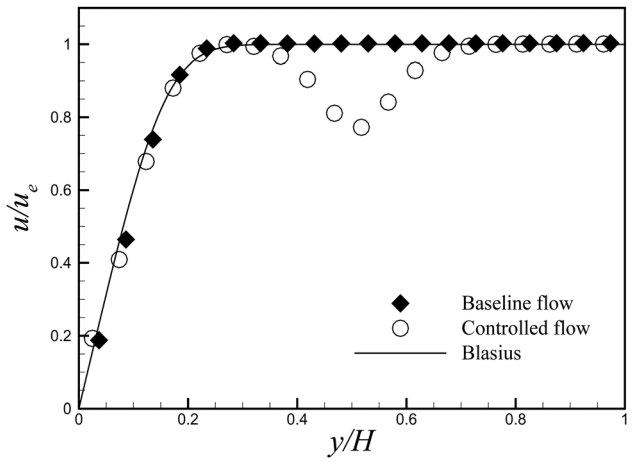

Fig. 2 Mean velocity profiles at the cavity leading edge for the baseline and the controlled flows

Results and Comment

Statistical Analysis. The profiles of the streamwise component of the mean velocity at different distances from the leading edge are reported in Fig. 3(*a*) for the baseline and the controlled flows. Reverse flow near the cavity bottom reveals for both flows the presence of the large clockwise recirculation zone in the downstream part of the cavity. A counterrotating bubble in the upstream part is poorly evidenced by the velocity profiles, but clearly discernible looking at the velocity streamline plots, not reported here. The wake of the cylindrical rod at $y/H = 0.5$ and the shear layer separating from the cavity leading edge are evident, showing the expected velocity defect. It is important to observe that the flow between the rod and the shear layer assumes a velocity nearly equal to the external velocity for more than 2/3 of the cavity length, suggesting the absence of direct interference between the cylinder wake and the shear layer in this region. As it is also confirmed by the profiles of the v component of the mean velocity in Fig. 3(*b*) the rod and its wake scarcely influence the mean velocity in the cavity and in the shear layer.

In order to understand if the presence of the rod deflects upward the shear layer, thereby impairing the efficiency of its interaction with the aft cavity wall, a measure of the shear layer deflection is reported in the next figure. The final position y_f (at $x/H = 2.9$) of the velocity streamlines, obtained by averaged velocity maps, as a function of the initial position y_i (at $x/H = 0.05$) is reported in Fig. 4 for different streamlines in the shear layer and above the cavity. The comparison between the two flows, the basic and the controlled one, does not show an evident lift-off of the shear layer induced by the rod.

The normalized standard deviations of the streamwise u' and bottom wall normal v' components of the fluctuating velocity are reported in Fig. 5 for the baseline flow and for the controlled flow.

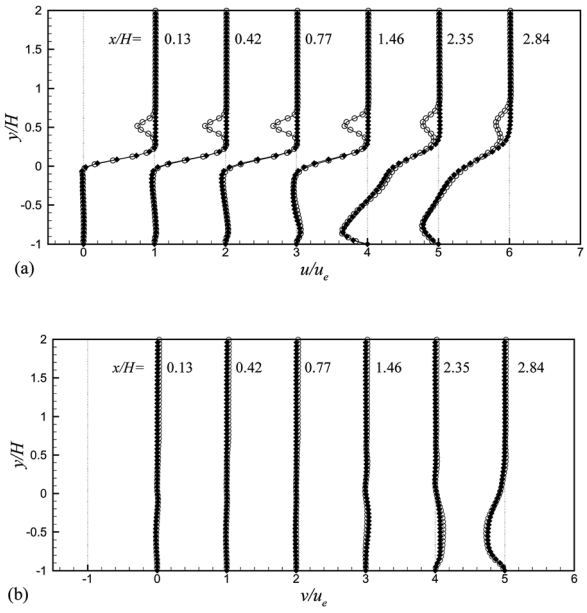

Fig. 3 Normalized streamwise (u/u_e) and bottom wall normal (v/u_e) mean velocity profiles at different distances from the leading edge. Each velocity profile is shifted by 1 with respect to the previous one. Plain symbols: baseline flow. Empty symbols: controlled flow.

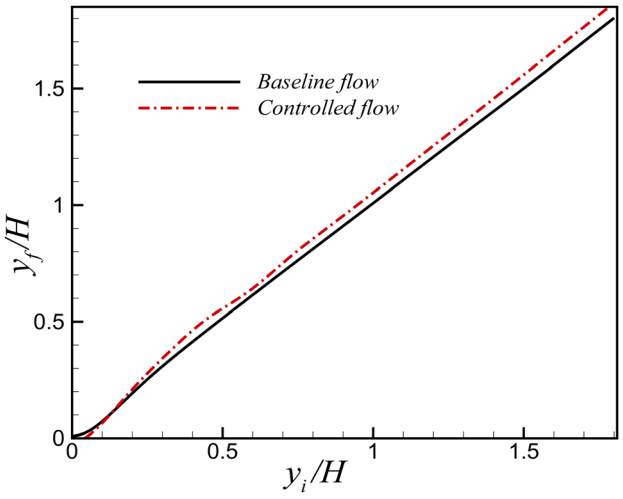

Fig. 4 Final position y_f of the streamlines at $x/H = 2.9$ as a function of the initial position y_i at $x/H = 0.05$

In Fig. 5 the differences between the controlled and the baseline flow fields are also reported for u' and v'. Large velocity fluctuations are observed in the downstream bubble zone, in the shear layer, and in the rod wake. Quiet flow is observable for both u' and v' velocity components in the upstream region, between the cavity mouth and the rod wake, where the mean velocity assumes values very close to the undisturbed velocity (Fig. 3). It may be observed that the velocity fluctuations in the rod wake decay going downstream, while they appear to be reinforced in the shear layer. Peaks of fluctuations of both velocity components are observed in the shear layer in the region between x/H =2 and x/H =3. A different behavior is observed for u' and v' in the shear layer of the baseline flow and of the controlled flow. While the peak value of u' increases of about 30% in the controlled flow with respect to the baseline case, the peak value of v' decreases of about 15%.

The increase of the longitudinal u'-velocity fluctuations is due to velocity induced by the vortices traveling in the rod wake. This is consistent with the fact that the observed increase of u' is more evident in the downstream region, where the rod wake interacts with the shear layer. The decrease of v' in the case of the controlled flow may be explained after examining the vorticity field.

In Fig. 6 the mean and the standard deviation of the spanwise normalized vorticity are reported for the baseline and the controlled flows. The differences between the two flows are also reported. High values of the mean vorticity ω are shown in the shear layer, in the rod wake, and in the downstream recirculating bubble. Anticlockwise (positive) vorticity are evidenced, near the aft wall, induced by the clockwise (negative) bubble. In both flows the absolute value of the mean vorticity in the shear layer assumes a peak value at about $x/H = 0.3$ in the proximity of the leading edge and then decays going downstream, assuming higher values in the case of the baseline flow. Actually, the distribution of the absolute value of the mean vorticity along the shear layer shows a reduction up to 20%, in the last 2/3 of the cavity shear layer, for the case of the controlled flow with respect to the basic flow. In the case of the controlled flow, the distribution of the vorticity standard deviation ω' along the shear layer shows an increase in the upstream region ($x/H \leq 1/3$) up to about 100% and a reduction up to 15% in the downstream region. The increase of ω' in the upstream region is due to the train of weak vortices traveling along the shear layer induced by the cylinder von Karman wake. The presence of these vortices will be highlighted in Fig. 7. The reduction of the mean spanwise component of the vorticity absolute value and of its standard deviation in the downstream region is provoked by the development of the rod wake. In fact it has been recently demonstrated by means of numerical simulations (Stanek et al. [10]) that the initial spanwise coherence and the successive breakdown of the pair of opposite sign vortical structures injected at high frequency by the rod lead to a reorganization of the vorticity field in the cavity shear layer. In particular, the vortical structures in the shear layer lose in part their spanwise coherence, already in the region close to the leading edge, showing consequently a new organization with their axis more often oriented in the y direction and in the x direction rather than in the z direction. This effect justifies, to a good extent, the measured reduction in the mean and fluctuating spanwise component of the vorticity in the case of the controlled flow in the shear layer region. Moreover, the reduction of the vorticity absolute value in the controlled shear layer can be in part attributed to an unwind action by the positive Karman vortices in the cylinder wake lower side, as it will be evidenced later. The early loss of spanwise coherence of the structures in the shear layer justifies also the observed reduction of the v' component of the fluctuating velocity shown in Fig. 5 for the case of controlled flow.

Considering the fact that the reorganization of the spanwise vorticity in the shear layer due to the high frequency vortex shedding from the cylinder may play an important role in the suppression of the cavity tone [10], ad hoc preliminary PIV experiments have been done in a plane (x,z) parallel to the cavity floor, at $y/H = 0.05$. The results are reported in the Appendix. The observation of the spanwise correlation analysis of the streamwise velocity in the plane (x,z) confirms the numerical results of Ref. [10], showing the dramatic loss of spanwise coherence already very close to the leading edge, in the case of the controlled flow. It should be recalled that Stanek et al. [10] affirm that this specific reorganization is responsible for the cavity tone suppression.

Instant Field and Velocity Spectra. Samples of snapshots visualizing instantaneous spanwise vortices are shown in Fig. 7. To detect vortical structures in the measurement plane, the λ_{ci} vortex identification criterion was used, where λ_{ci} is the swirling strength as introduced by Zhou et al. [16]. The same methodology was applied by Haigermoser et al. [17] in their investigation of a cavity flow with a thick incoming turbulent boundary layer. Clockwise vortices, due to Kelvin-Helmholtz instability, are identified in the shear layer of the baseline flow. By the visual observation of the time resolved sequence of snapshots like the one in Fig. 7(*a*), in the baseline flow, the vortices are seen to grow up going downstream inside the shear layer. They start to be observable at about $x/H = 1$ and then are convected downstream with a well identifiable constant periodicity. Simply from the visual analysis of the time resolved sequence of snapshots, counting the number of vortices going through a given point in the shear layer, a uniquely individuated frequency of 10 Hz (St = 1) is easily measured.

The time resolved snapshots of the controlled flow show a very regular shedding of vortices (von Karman wake) downstream the rod, at the expected frequency of 77.5 Hz (St = 7.5), about one order of magnitude higher than the frequency of the vortices shed in the shear layer of the baseline flow. A sequence of weaker vortices is also visible in the controlled shear layer, starting upstream the cavity leading edge. They are seen to be highly correlated with the vortices shed by the rod and to travel at the same speed. Going downstream in the shear layer these vortices are weakened and new stronger vortices start to be visible in the region behind $x/H \cong 2$ at a not uniquely individuated frequency. They appear strongly disturbed by the structures re-emitted in the shear layer from the downstream recirculating flow inside the cavity and by the cylinder von Karman wake. The formation of these vortices does not shows constant periodicity, as in the case of the baseline flow. Furthermore, from the time resolved sequence of snapshots, like the one in Fig. 7(*b*), it is observed an unwind action by the positive Karman vortices in the cylinder lower wake, causing a weakening of the (irregular) shear layer vortices.

The description of the flow behavior, previously given on the base of the visual observation of the time resolved snapshot

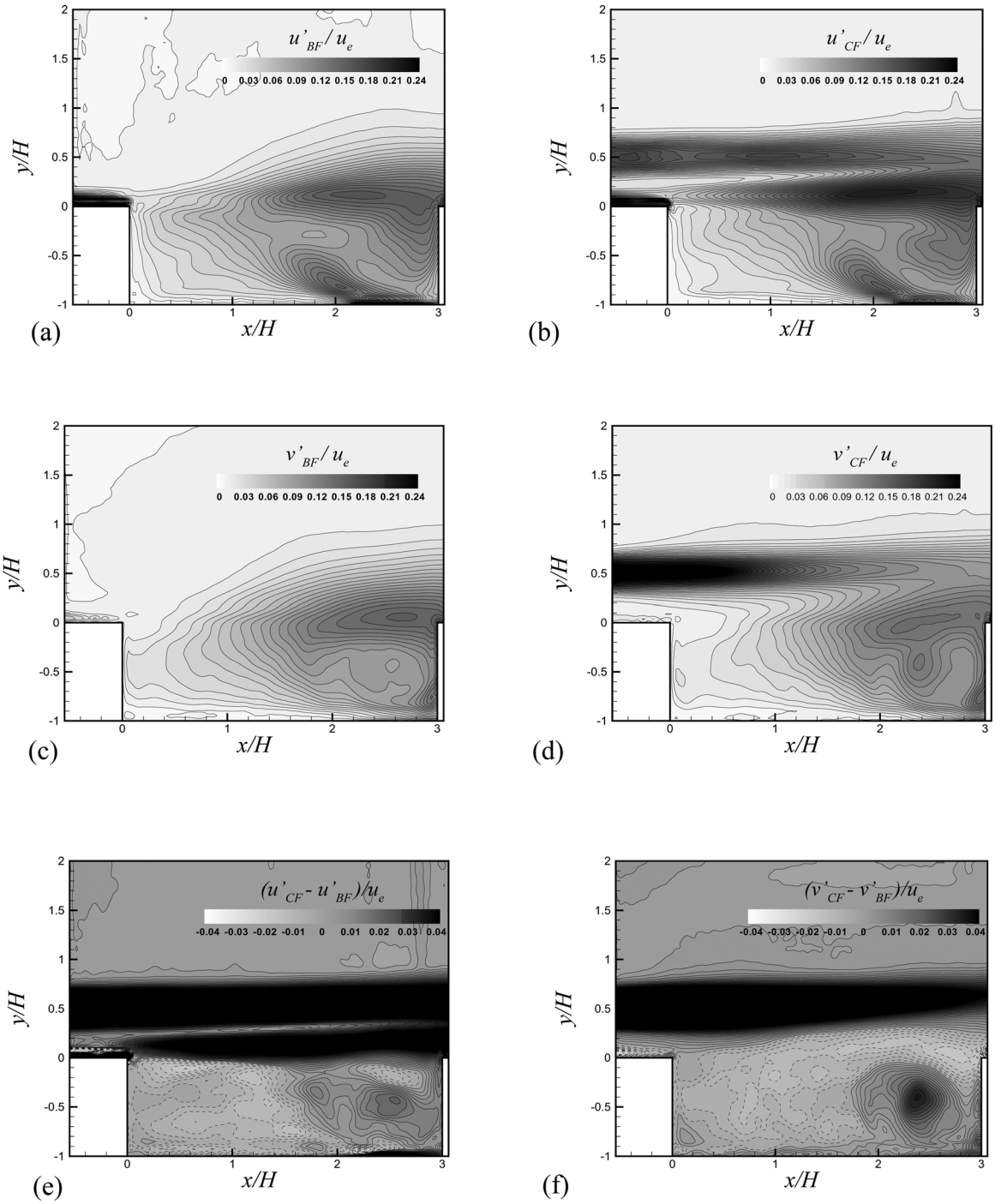

Fig. 5 Normalized standard deviation of the streamwise fluctuating velocity: (*a*) baseline flow u'_{BF}/u_e; (*b*) controlled flow u'_{CF}/u_e. Normalized standard deviation of the bottom wall normal fluctuating velocity: (*c*) baseline flow v'_{BF}/u_e; (*d*) controlled flow v'_{CF}/u_e. (*e*) → (*b*)–(*a*); (*f*) →(*d*)–(*c*). Dashed lines indicate negative values.

sequences, is quantitatively highlighted in Fig. 8 by the power spectral density P_v of the bottom wall normal component of the velocity, computed along the cavity mouth. In order to highlight small amplitude values of the power spectrum, P_v is diagrammed in logarithmic scale for the first two measurement positions. At $x/H = 0.24$, very near the cavity leading edge, the two spectra, for the baseline and the controlled flows, show a very small energy content peak at low frequency, around Strouhal number equal one. The remaining part of the spectrum appears to be flat for the baseline flow, while a small peak is present in the case of the controlled flow at $\mathrm{St} = 7.5$, corresponding to the frequency of the von Karman vortex shedding from the cylindrical rod. This peak appears greatly reduced already at $x/H = 0.75$ and it is not visible in the further downstream measurement positions. This is consistent with the visual observation of the sequence of images like the one in Fig. 7(*b*) for the controlled flow, where the shown vortices traveling in the shear layer of the cavity leading edge region, highly correlated with the von Karman cylindrical wake, decay going downstream. Observing the downstream spectra, from $x/H = 1.2$, a narrow peak of P_v starts to be visible for the case of the baseline flow, at $\mathrm{St} = 1$, increasing in amplitude going toward the cavity trailing edge. The frequency of this discrete tonal peak corresponds to the second mode predicted by the Rossiter formula, $\mathrm{St} = 0.997$ ($\gamma = 0.25$ and $k = 0.57$, as suggested by Rossiter [1]). A

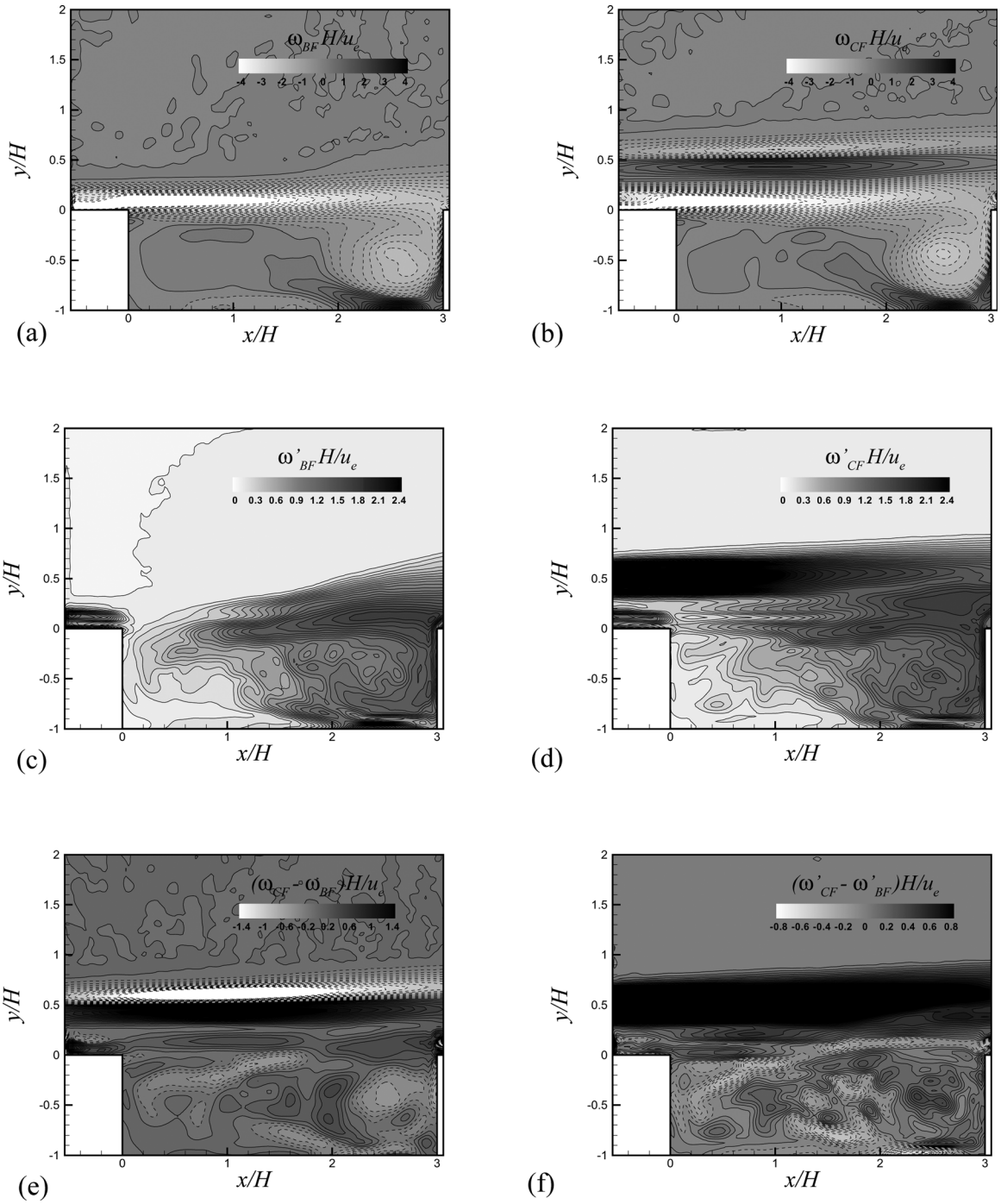

Fig. 6 Normalized mean vorticity: (*a*) baseline flow $\omega_{BF}H/u_e$; (*b*) controlled flow $\omega_{CF}H/u_e$. Normalized vorticity standard deviation: (*c*) baseline flow $\omega'_{BF}H/u_e$; (*d*) controlled flow $\omega'_{CF}H/u_e$. (*e*) → (*b*)–(*a*); (*f*) → (*d*)–(*c*). Dashed lines indicate negative values.

small peak also starts to be observable, at about St = 1.6, in the downstream locations. This value is very close to the one given by the Rossiter formula for the third mode, St = 1.567.

The discrete tonal peak present in the velocity spectra of the baseline flow appears to be suppressed in the controlled flow, where the spectra show only a low amplitude broadened peak around St = 1. This broadened peak is due to the transit of vortices at a not uniquely individuated frequency, as previously pointed out in the description of the time resolved sequence [see Fig. 7(*b*)].

A comment should be done about the fact that in the baseline flow the tonal frequency has been found to correspond to the second mode predicted by the Rossiter formula. Sarpotdar et al. [14] showed a comparison between experimentally observed Strouhal number of the dominant instability associated with cavity tones in their experiments on a cavity with $L/H = 2$ and the prediction of the Rossiter formula. It appears from the comparison (Fig. 4 of their paper) that at high Mach number their experimental data are in good agreement with the theoretical prediction, showing a tonal frequency corresponding to the first mode predicted by the Rossiter formula, with $k = 0.75$ and $\gamma = 0.30$. However, at very low Mach numbers, $M < 0.3$, the experimental cavity tone frequency shifts to a value very close to the one corresponding to the second mode predicted by Rossiter. Similar behavior was observed by Gharib and Roshko [2] in their experimental investigation of incompressible flow over an axisymmetric cavity. The authors observed that the cavity oscillates in mode II or mode III, always

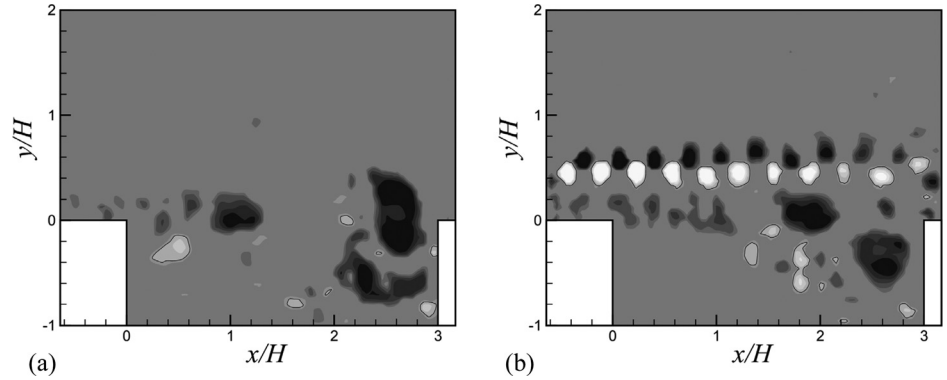

Fig. 7 Visualization of the instantaneous swirling strength. (*a*) Basic flow and (*b*) controlled flow. Dark gray: clockwise vortices (negative). Light gray: counterclockwise vortices (positive). More intense gray levels correspond to stronger vortices.

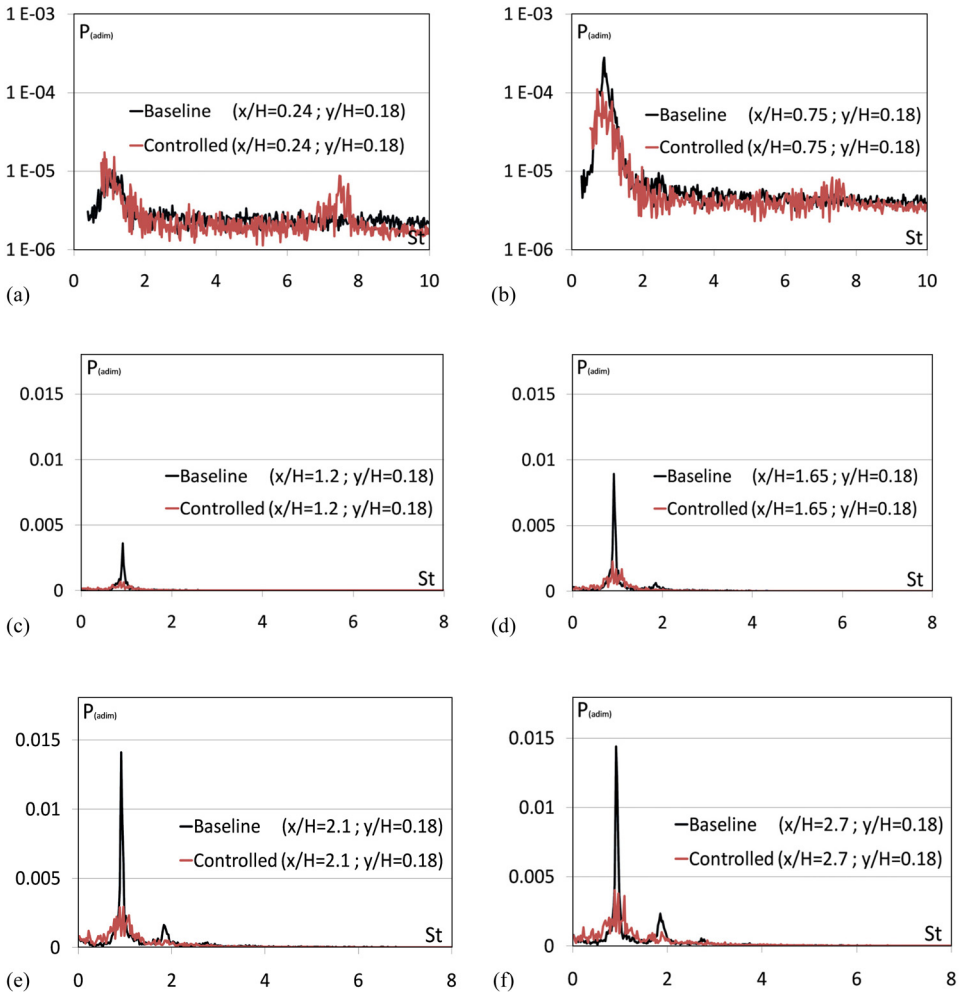

Fig. 8 Normalized power spectral density $P_{(adim)} = P_v/(u_e H)$ of the bottom wall normal component of the velocity along the cavity mouth, at different distances from the leading edge. Black line: baseline flow. Gray line: controlled flow.

omitting the first mode. These results appear to be in agreement with the present low Mach number measurements.

It should be noticed that the nature of the self-sustained oscillations in cavities at very low Mach numbers has been object of debate. Tam and Block [18] claimed that at very low Mach numbers the cavity physics is dominated by normal mode resonance. If this were the case, their model would predict, in the present experiment, oscillations at very much higher frequency (see Fig. 18 in their paper). More recently Chatellier et al. [19] argued that the self-sustained oscillations, in very low subsonic flows, can be a direct consequence of the natural instability of the cavity shear layer, strongly enhanced by the presence of the cavity downstream edge. In this case, the feedback process is a quasi immediate consequence of the hydrodynamic disturbance occurring at the downstream edge. This mechanism was defined as a fluid-dynamic oscillation mode in the Rockwell and Naudascher review [20],

where the Rossiter mechanism was defined as a longitudinal fluid-resonant mode.

Finally, it should be observed that the cavity flow is a complicated dynamical system and, due to the amount of geometrical and physical parameters involved, the mechanism of self-sustained oscillations is not yet completely characterized. Although the object of the present work was not to speculate on the nature of the self-sustained oscillations in a very low Mach number cavity flow, a valuable contribution comes out from the present space and time resolved measurements. Vortical structures have been detected traveling in the shear layer of the baseline flow towards the trailing edge with a well individuated discrete frequency (the St = 1 tonal peak in the velocity spectrum), corresponding to the second mode predicted by the Rossiter formula. Moreover, a second smaller peak can be observed in the velocity spectrum at a frequency very close to the third Rossiter mode.

Stability Analysis. In order to try to understand how the modification of the baseline flow produced by the control affects the stability characteristics of the shear layer, a linear stability analysis has been performed on the experimentally measured shear layer mean velocity profiles downstream the cavity leading edge. In order to apply the classical Orr-Sommerfeld equation, the flow has been assumed to be locally parallel. This assumption is justified by the fact that in the shear layer and in the von Karman wake the ratio between the y component and x component of the mean velocity does not exceed 7% in the region where the stability analysis is applied. Locally higher values are present inside the cavity.

The Orr-Sommerfeld equation has been numerically solved by means of a fourth-order finite difference method in the computational domain $-H \leq y \leq y_{\max}$, with $y_{\max}$ six times larger than the boundary layer thickness. At $y = -H$ the physical no-slip boundary conditions have been applied, while at $y = y_{\max}$ a free-stream condition has been imposed. The time amplification coefficients c_i obtained from the numerical solution have been then transformed into spatial amplification factors α_i by means of the following relation [21]:

$$\alpha_i = -\frac{\bar{k} c_i}{\dfrac{\partial \omega}{\partial \bar{k}}}$$

where ω is the pulsation and $\bar{k}$ is the wavenumber. Figure 9 shows the resulting spatial amplification factor, normalized with the cavity depth H, as a function of the Strouhal number, for three sections downstream the cavity leading edge.

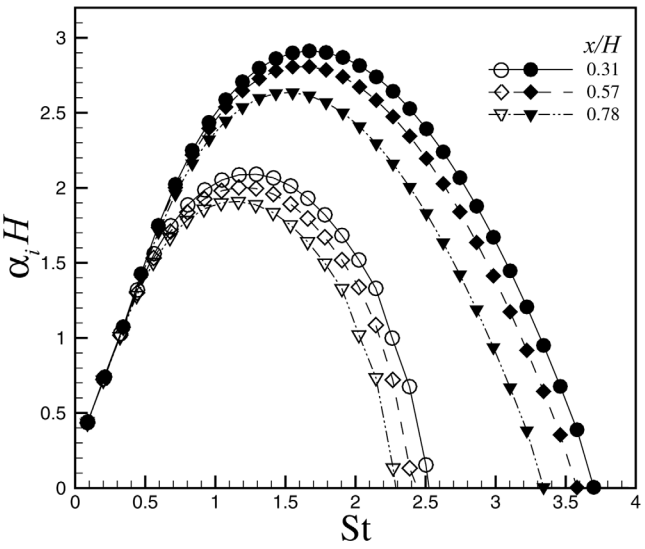

Fig. 9 Dimensionless spatial amplification factor as function of the Strouhal number. Plain symbols: baseline flow. Empty symbols: controlled flow.

A first observation is that the presence of the rod does not alter significantly the stability characteristics of the shear layer; namely, the spatial amplification factor and the range of unstable frequencies are only slightly reduced by the control. An important find is that the instability corresponding to the second Rossiter mode at St = 1 lies within the envelope of the most amplified frequencies, conversely the Strouhal number corresponding to the vortex shedding frequency from the rod (St = 7.5) lies well outside the amplification envelope in the region where there is no spatial growth of the instability modes. Thus, disturbances in the shear layer at the rod von Karman shedding frequency, according to the linear stability theory, are expected to decay in the streamwise direction. This is in agreement with what is observed analyzing the time resolved sequences of snapshots, like the one in Fig. 7, and with the results of the spectral analysis of the y component of the velocity in the shear layer (Fig. 8).

Moreover, the time resolved sequences have shown that irregularly generated vortices of considerable intensity take form downstream in the shear layer, in the region close to the cavity trailing edge, also in the case of the controlled flow [see Fig. 7(*b*)]. These large structures produced by the Kelvin-Helmholtz hydrodynamic instability can still be amplified because the range of unstable frequencies is only slightly reduced by the control.

Drag Analysis. Further information about the behavior of the baseline and controlled flow inside the cavity may be deduced from a global analysis, looking at the instantaneous flow momentum flux through the cavity mouth or looking at the associated drag applied to the cavity wall. Assuming that the presence of the cavity does not influence the flow upstream and downstream, the momentum balance applied to the flow inside the cavity gives the relation between the drag force on the cavity walls and the momentum flux across the cavity mouth. The instantaneous drag per unit spanwise length is given by Haigermoser et al. [17]:

$$D(t) = \int_{(\text{c.m.})} \left(-\rho uv + \mu \frac{\partial u}{\partial y} \right) dl$$

where u and v are the instantaneous component of the velocity and the momentum flux and the shear stress are integrated along the cavity mouth (c.m.).

In Fig. 10 the instantaneous cavity drag coefficient $C_D(t) = 2D/(\rho u_e^2 H)$ is displayed as a function of time for the baseline and the controlled flows. These time histories show the global unsteady nature of the two flows in the measurement plane. Instants of negative drag are present in the two time histories. Examining the baseline flow, a drag fluctuation of relatively high frequency, around 10 Hz, superimposed to a lower frequency fluctuation of larger amplitude appears evident. It is difficult to characterize quantitatively this low frequency oscillation, due to the shortness of the recorded time histories, limited to 3.2 s each. Approximately from two to four oscillations are observed in each time history, like the one in Fig. 10 for the baseline flow. The lower frequency oscillation may be tentatively attributed to a kind of flapping motion involving the whole cavity shear layer. This low frequency oscillation is also present in the case of the controlled flow with about comparable frequency and amplitude.

The observed higher frequency of about 10 Hz (St = 1) corresponds to the frequency of the second Rossiter mode and it is attributable to the dynamics of the vortical structures along the cavity mouth. High frequency oscillations are also observable in the drag time histories for the controlled flow, but they are of smaller amplitude and they show considerable variation in frequency.

In order to visualize the flow in instants of high and low drag, a conditional average of the flow fields based on $C_D > C_{D,\text{mean}} + C_{D,\text{rms}}$ and $C_D < C_{D,\text{mean}} - C_{D,\text{rms}}$ was performed, leading to the flow configurations in Fig. 11. It is clearly noticed for both

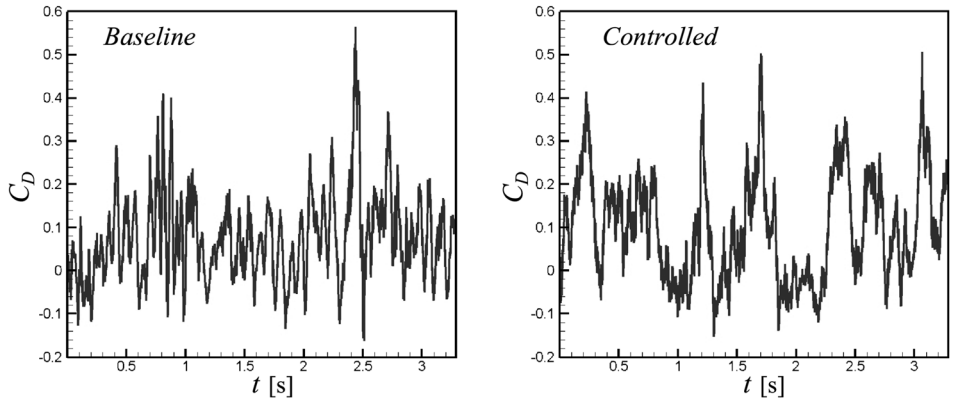

Fig. 10 Instantaneous cavity drag coefficient per unit spanwise length in function of time (seconds)

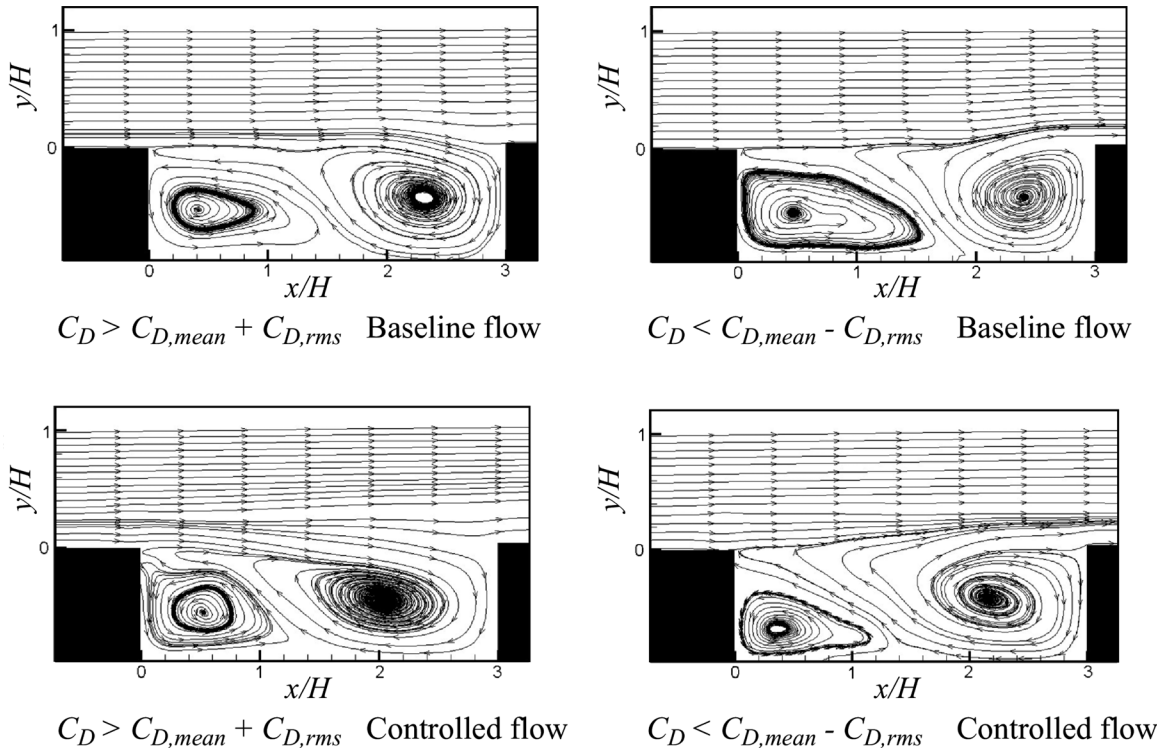

Fig. 11 Conditional averaged streamlines

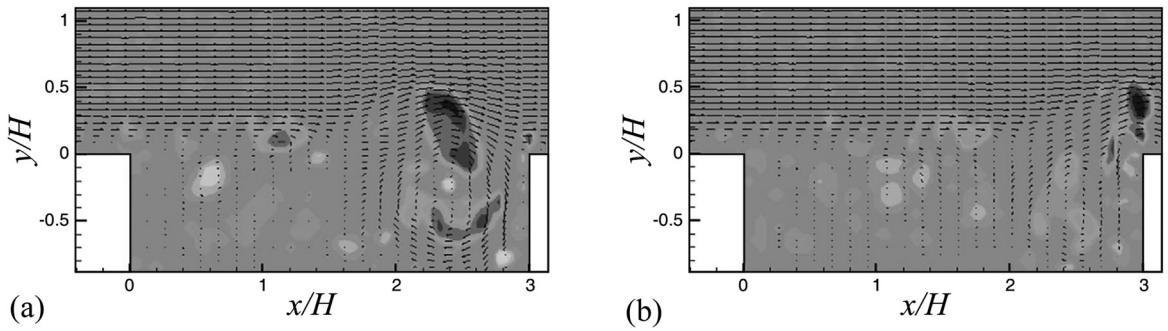

Fig. 12 Instantaneously detected vortices superimposed to the velocity field for the baseline flow

the baseline and the controlled flows that instants of high drag are connected with an inflow into the cavity, whereas instants of low drag are connected with outflow. Howe [22] also found such a relation between cavity oscillations and the drag. In the case of controlled flow the primary recirculation zone appears enlarged. For both flows the mean detachment point of the backward flow on the bottom wall is moved closer to the leading edge in the case of inflow and the shear layer impinges onto the top of

the forward facing step, while it jumps over the cavity in the case of outflow.

It has been previously observed that the drag oscillations, and consequently the inflow-outflow processes, are due to the dynamics of the vortical structures along the cavity mouth.

PIV measurements allow us to visualize this process. In Fig. 12 instantaneous detected vortices are shown superimposed to the velocity field for the baseline flow. Figure 12(*a*) refers to an instant of high drag (inflow) and Fig. 12(*b*) refers to an instant of low drag (outflow). It is clearly seen that outflow takes place when the vortex jumps over the trailing edge; conversely inflow takes place when the vortex is approaching the trailing edge. Similar oscillating behavior is observed in the case of the controlled flow, not shown here.

Shear layer oscillating behavior is also described by Ukeiley and Murray [23]. They demonstrated the pumping action occurring in an open cavity (with $L/H = 5.16$ and subsonic flow $M = 0.2$), showing cycles of inhalation phase followed by exhalation phase. They observed that the pumping cycles are driven by a build up of fluid beneath the shear layer.

Finally, the observed inflow and outflow oscillations and flow continuity suggest for the baseline and the controlled the existence of a transversal periodic motion. This is highlighted also by the spiral nature of the primary recirculating bubbles in Fig. 11.

Conclusions

Time resolved PIV measurements have been applied to nominally 2D cavity flows having the ratio length-to-depth $L/H = 3$. The primary objective was to contribute to the understanding of the physics governing the suppression mechanism of the cavity flow self-sustained oscillations by means of a cylindrical rod positioned transversally just upstream the cavity entrance. The rod was positioned at the external edge of the incoming boundary layer. The present measurements confirm the effectiveness of this device for the cavity self-sustained oscillations suppression.

As reported in the Introduction, several physical mechanisms have been hypothesized to explain the cavity tone suppression resulting from the use of the cylinder in cross flow. The most accredited mechanisms are that the suppression is due (a) to the lifting-off of the shear layer, (b) to the altered stability characteristics of the shear layer, (c) to a specific reorganization of the vorticity in the shear layer due to the spanwise breakdown of the initially spanwise coherent pair of counterrotating vortices in the cylinder wake, and (d) to a disturbance effect provoked by the direct interaction of the cylinder wake with the shear layer.

It has to be expected that various causes may simultaneously concur to the cavity tone suppression by the rod in cross flow, but the present experimental results almost exclude contributions to the observed tone suppression by the first two mechanisms (a) and (b). The result in Fig. 4 does not show evident lift-off of the shear layer induced by the rod to justify the cavity tone suppression. The result in Fig. 9 shows that the presence of the rod does not alter significantly the stability characteristics of the shear layer. Namely, the spatial amplification factor and the range of unstable frequencies are only slightly reduced by the control.

About the third mechanism the present results show that a rearrangement of the vorticity field takes place, due to the presence of the rod, producing reduction of the spanwise coherence of the vortical structures in the shear layer. As observed by Stanek et al. [10], this vorticity reorganization is in the direction of more random field; therefore pushing the flow toward stability and contributing to the cavity tone suppression. In addition, the results in Figs. 5 and 6 show that a direct interaction between the cylinder wake and the shear layer takes place in the region near the cavity trailing edge. It may be argued that this interaction also contributes to a less two-dimensional organized motion of the vortices in the shear layer and to the reduction of the negative vorticity in the shear layer due to an expected unwind action by the positive Karman vortices in the cylinder wake lower side.

The scenario which appears from the present results for the controlled flow is the following. The high frequency excitation, due to the unsteady wake of the cylindrical rod, controls an instability process in the shear layer, near the leading edge, by forcing it at a frequency corresponding to the von Karman vortex shedding frequency (Fig. 7). As shown by the stability analysis and as found by Panickar and Raman [13], this high frequency excitation lies outside the envelope of the amplified instabilities (Fig. 9) then decays rapidly as it is convected downstream along the shear layer (Fig. 8). Moreover, vortical disturbances at a frequency of the order of the tone frequency for the baseline flow, appear in the controlled shear layer from about 2/3 of the cavity and are amplified going downstream (Figs. 7 and 8). These vortices, possibly due to the previously mentioned mechanisms (c) and (d), do not show the regular behavior expected in the case of self-sustained oscillation conditions, as in the case of the uncontrolled flow. They give rise only to a modest broadened peak in the velocity spectra (Fig. 8).

A global analysis of the flow field by looking at the cavity instantaneous drag per unit span shows for the baseline flow a drag fluctuation of relatively high frequency superimposed to a lower

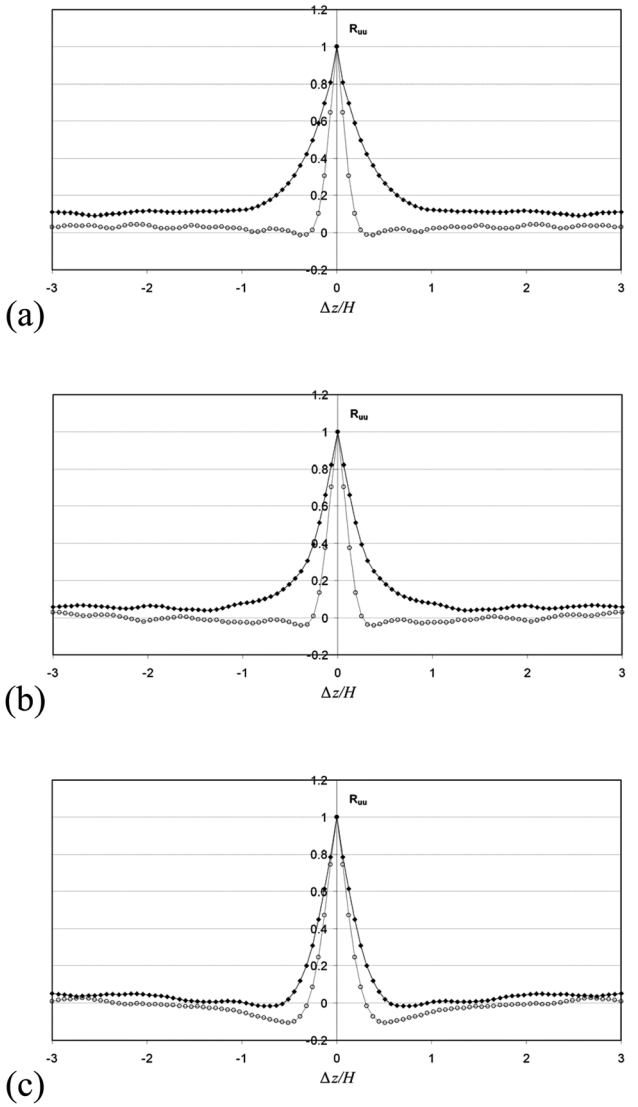

Fig. 13 Spanwise autocorrelation function of the streamwise component of the velocity at $y/H = 0.05$ and at different distances from the cavity leading edge. Plain symbols: baseline flow. Empty symbols: controlled flow. (*a*) $x/H = 0.4$; (*b*) $x/H = 1.1$; and (*c*) $x/H = 2.9$.

frequency fluctuation of larger amplitude. The observed high frequency corresponds to the frequency of the cavity tone ($St = 1$) and it has been attributed to the dynamics of the vortical structures along the cavity mouth. The approaching of a vortical structure to the trailing edge induces inflow, causing high drag, conversely a vortical structure passing the trailing edge induces outflow, causing low drag. A similar process is observed for the controlled flow, but the drag oscillations show considerable variation in frequency and appear to be of smaller amplitude with respect to the one in the baseline flow.

The low frequency oscillation has been tentatively attributed to a kind of flapping motion involving the whole cavity shear layer. This low frequency oscillation is also present in the case of the controlled flow with comparable frequency and amplitude.

Appendix

Results of a preliminary PIV experiment performed in the plane (x,z) parallel to the cavity floor at $y/H = 0.05$ are reported in this Appendix. The flow conditions are the same of the PIV measurements in the plane (x,y), reported in Table 1.

The spanwise autocorrelation function of the streamwise component of the velocity R_{uu} at different distances from the cavity leading edge, is shown in Fig. 13. Near the leading edge and at about half cavity length, the correlation R_{uu} shows for the controlled flow a much smaller spanwise integral scale with respect to the case of the baseline flow, while near the trailing edge the scales of the two flows appear comparable.

References

[1] Rossiter, J. E., 1966, "Wind Tunnel Experiments on the Flow Over Rectangular Cavities at Subsonic and Transonic Speeds," Technical Report No. 3438, Aeronautical Research Council Reports and Memoranda, London.

[2] Gharib, M., and Roshko, A., 1987, "The Effect of Flow Oscillations on Cavity Drag," J. Fluid Mech., **177**, pp. 501–530.

[3] Sarohia, V., 1977, "Experimental Investigation of Oscillations in Flows Over Shallow Cavities," AIAA J., **15**, pp. 984–991.

[4] Rowley, C. W., and Williams, D. R., 2006, "Dynamics and Control of High-Reynolds-Number Flow Over Open Cavities," Annu. Rev. Fluid Mech., **38**, pp. 251–276.

[5] Cattafesta, L., Williams, D. R., Rowley, C. W., and Alvi, F., 2003, "Review of Active Control of Flow-Induced Cavity Resonance," AIAA Paper No. 2003-3567.

[6] McGrath, S. F., and Shaw, L. L., 1996, "Active Control of Shallow Cavity Acoustic Resonance," AIAA Paper No. 96-1949.

[7] Shaw, L. L., 1998, "Active Control for Cavity Acoustics," AIAA paper No. 98-2347.

[8] Stanek, M. J., Raman, G., Kibens, V., Ross, J. A., Odedra, J., and Peto, J. W., 2001, "Suppression of Cavity Resonance Using High Frequency Forcing—The Characteristics Signature of Effective Devices," AIAA Paper No. 2001-2128.

[9] Stanek, M. J., Raman, G., Ross, J. A., Odedra, J., Peto, J., Alvi, F., and Kibens, V., 2003, "High Frequency Acoustic Suppression—The Mystery of the Rod-in-Crossflow Revealed," AIAA Paper No. 2003-0007.

[10] Stanek, M. J., Visbal, M. R., Rizzetta, D. P., Rubin, S. G., and Khosla, P. K., 2007, "On a Mechanism of Stabilizing Turbulent Free Shear Layers in Cavity Flows," Comput. Fluids, **36**, pp. 1621–1637.

[11] Smith, B., Welteren, T., Maines, B., Shaw, L,. Stanek, M., and Grove, J., 2002, "Weapons Bay Acoustic Suppression From Rod Spoilers," AIAA Paper No. 2002-0662.

[12] Ukeiley, L., Ponton, M. K., Seiner, J. M., and Jansen, B., 2002, "Suppression of Pressure Loads in Cavity Flows," AIAA Paper No. 2002-0661.

[13] Panickar, P., and Raman, G., 2008, "Cavity Resonance Suppression Using High Frequency Excitation: The Mystery of the Cylinder-in-Crossflow Revisited," AIAA Paper No. 2008-2853.

[14] Sarpotdar, S., Panickar, P., and Raman, G., 2010, "Stability of a Hybrid Mean Velocity Profile and Its Relevance to Cavity Resonance Suppression," Phys. Fluids **22**, p. 076101.

[15] Raffel, M., Willert, C. E., Wereley, S. T., and Kompenhans, J., 2007, *Particle Image Velocimetry—A Practical Guide*, Springer, Berlin.

[16] Zhou, J., Adrian, R. J., Balachandar, S., and Kendall, T. M., 1999, "Mechanisms for Generating Coherent Packets of Hairpin Vortices in Channel Flow," J. Fluid Mech., **387**, pp. 353–396.

[17] Haigermoser, C., Vesely, L., Novara, M., and Onorato, M., 2008, "A Time Resolved Particle Image Velocimetry Investigation of a Cavity Flow With a Thick Incoming Turbulent Boundary Layer," Phys. Fluids, **20**, p. 105101.

[18] Tam, C. K. W., and Block, P. J. W., 1978, "Tones and Pressure Oscillations Induced by Flow Over Rectangular Cavities," J. Fluid Mech., **89**, pp. 373–399.

[19] Chatellier, L., Laumonier, J., and Gervais, Y., 2006, "Theoretical and Experimental Investigations of Low Mach Number Turbulent Cavity Flows," Exp. Fluids, **36**, pp. 728–740.

[20] Rockwell, D., and Naudascher, E., 1978, "Review: Self-Sustained Oscillations of Flow Past Cavities," ASME J. Fluids Eng., **100**, pp. 152–165.

[21] Drazin, P. G., and Reid, W. H., 1981, *Hydrodynamical Instability*, Cambridge University Press, Cambridge.

[22] Howe, M. S., 1997, "Low Strouhal Number Instabilities of Flow Over Apertures and Wall Cavities," J. Acoust. Soc. Am., **102**, pp. 772–780.

[23] Ukeiley, L., and Murray, N., 2005, "Velocity and Surface Pressure Measurements in an Open Cavity," Exp. Fluids, **38**, pp. 656–671.